JACS
JOURNAL OF THE AMERICAN CHEMICAL SOCIETY
Article
pubs.acs.org/JACS

Transition from Superlithiophobicity to Superlithiophilicity of Garnet Solid-State Electrolyte

Wei Luo,[†,‡,⊥] Yunhui Gong,[†,§,⊥] Yizhou Zhu,[†,§] Kun Kelvin Fu,[†,§] Jiaqi Dai,[†,§] Steven D. Lacey,[†,§] Chengwei Wang,[†,§] Boyang Liu,[†,§] Xiaogang Han,[†,§] Yifei Mo,[†,§] Eric D. Wachsman,*[,†,§] and Liangbing Hu*[,†,§]

[†]Department of Materials Science and Engineering, [‡]Department of Mechanical Engineering, and [§]University of Maryland Energy Research Center, University of Maryland, College Park, Maryland 20742, United States

Supporting Information

ABSTRACT: All-solid-state Li-batteries using solid-state electrolytes (SSEs) offer enhanced safety over conventional Li-ion batteries with organic liquid electrolytes due to the nonflammable nature of SSEs. The superior mechanical strength of SSEs can also protect against Li dendrite penetration, which enables the use of the highest specific capacity (3861 mAh/g) and lowest redox potential (−3.04 V vs standard hydrogen electrode) anode: Li metal. However, contact between the Li metal and SSEs presents a major challenge, where a large polarization occurs at the Li metal/SSE interface. Here, the chemical properties of a promising oxide-based SSE (garnet) changed from "super-lithiophobicity" to "super-lithiophilicity" through an ultrathin coating of amorphous Si deposited by plasma-enhanced chemical vapor deposition (PECVD). The wettability transition is due to the reaction between Li and Si and the in situ formation of lithiated Si. As a result, symmetric cells composed of a Si-coated garnet-structured SSE and Li metal electrodes exhibited much smaller impedance and excellent stability upon plating/stripping cycles compared to cells using bare garnet SSE. Specifically, the interfacial resistance between Li and garnet dramatically decreased from 925 to 127 Ω cm^2 when lithiated Si was formed on the garnet. Our discovery of switchable lithiophobic-lithiophilic surfaces to improve the Li metal/SSE interface opens opportunities for improving many other SSEs.

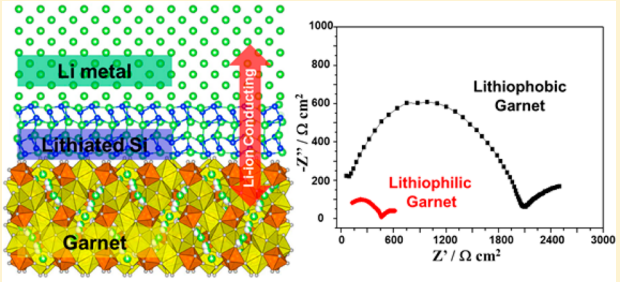

Transition from Super-lithiophobicity to Super-lithiophilicity of Garnet leads to a much smaller interfacial resistance

INTRODUCTION

Since the commercialization of Li-ion batteries (LIBs) in the 1990s, they have attracted great interest and now dominate the market for powering commercial electronics such as smart phones and laptops.[1,2] This successful battery technology depends to a great extent on the use of graphite-based anodes. However, Li metal itself is the optimal anode because it is lighter and offers the lowest potential (−3.04 V vs standard hydrogen electrode) and highest specific capacity (3861 mAh/g).[3,4] To date, well-known challenges with Li metal anodes still remain: (i) safety issues associated with the formation of Li dendrites, (ii) unstable solid electrolyte interphase (SEI) due to the highly reactive nature of Li metal, and (iii) low Coulombic efficiency upon cycling.[5] To circumvent these problems, numerous strategies were employed, including optimizing electrolyte components,[6,7] fabricating an artificial SEI,[8,9] minimizing the local current density,[10,11] building a scaffold structure,[12,13] and using advanced separators.[14] These strategies have presented great progress; however, safety concerns still exist due to potential Li dendrite growth and highly combustible organic electrolytes.

Solid-state electrolytes (SSEs), on the basis of fast ion conductors, are recognized as an all-encompassing concept to solve the Li metal anode problems.[15−17] For example, Li dendrites cannot penetrate through SSEs due to their superior mechanical strength.[18,19] Even during failure of all-solid-state Li batteries (ASSLBs), such as short circuiting, the nonflammable nature of SSEs would prevent dangerous fires or explosions from occurring. Moreover, many SSEs have shown great stability against Li metal even with the formation of SEI. Therefore, intensive efforts to develop SSEs are being pursued.[20−23] Among various SSEs, garnet-type materials are attractive.[24] In particular, $Li_7La_3Zr_2O_{12}$, a type of garnet, has exhibited superior Li-ion conductivity, a wide potential window, as well as high thermal and chemical stability since its discovery by Murugan et al. in 2007.[25] ASSLBs composed of a garnet SSE, a high voltage cathode, and a Li metal anode have stimulated research interest due to their safety, high energy/power density, and long cycle life. Unfortunately, the large interfacial resistance between the electrodes and the garnet largely has hampered their development.[26,27] As pointed out by Luntz and co-workers in their Viewpoint, minimizing the interfacial resistance between the SSEs and the electrodes should be more critical than maximizing the bulk ionic conductivity of SSEs for electric vehicle applications.[28]

Received: July 5, 2016
Published: August 28, 2016

DOI: 10.1021/jacs.6b06777
J. Am. Chem. Soc. 2016, 138, 12258−12262

To date, some efforts have been devoted to improving the cathode/garnet interface.[29,30] Among various technologies, doping or elemental substitution in garnet demonstrated improvement.[30,31] Recently, Kato and co-workers reported that the interface between garnet and the $LiCoO_2$ cathode could be greatly improved by growing a thin layer of niobium (Nb) on the garnet prior to $LiCoO_2$ deposition.[32] Their results suggested that an amorphous Li−Nb−O layer was formed in situ, which significantly lowered the $LiCoO_2$/garnet interfacial resistivity. Although this breakthrough has been reported on the cathode side, the interface between the Li metal anode and garnet SSE still presents a major challenge due to the "lithiophobic" nature of the garnet. Currently, vacuum evaporation or high pressure processes are used to deposit the Li metal anode onto garnet to minimize interfacial resistance, which greatly limits technological applications.[32−34]

The fundamental problem of poor contact between the Li metal and garnet is due to the high stability of garnet against Li metal. Recently, several strategies have been reported to improve the wettability of materials with Li metal, where a reaction between the Li metal and these materials is key.[12,13] Inspired by these works, we engineered the surface of garnet by coating an ultrathin layer of amorphous Si, which is known to be a highly reactive material, with Li. Through plasma-enhanced chemical vapor deposition (PECVD), the ultrathin (∼10 nm) amorphous Si coating layer can create perfect contact with the garnet. In this case, molten Li can wet the garnet rapidly (up to 4 s). Our experiments and theoretical calculations indicate that the reaction between Si and Li are crucial for enhanced wettability, which causes the garnet surface to switch from "superlithiophobic" to "superlithiophilic" behavior (Figure 1a and b). Moreover, lithiated Si was in situ

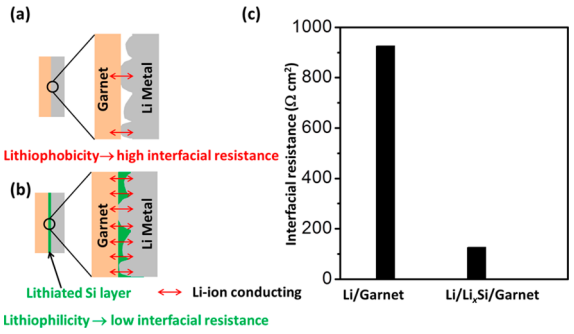

Figure 1. (a) Lithiophobic garnet has poor contact with Li metal, which leads to a high interfacial resistance. (b) The wettability of garnet is significantly improved due to the reaction between Li and Si and the in situ-formed, lithiated Si can act as a Li-ion conducting layer. (c) The wettability transition and the in situ-formed, lithiated Si lead to the dramatic decrease of garnet/Li metal interfacial resistance from 925 Ω cm^2 (bare garnet) to 127 Ω cm^2 (Si-coated garnet).

formed between garnet and Li metal, which acts as a Li-ion conductor layer; thus, symmetric cells using the lithiophilic garnet showed a much smaller interfacial resistance compared to that of the lithiophobic garnet (Figure 1c). We believe that our method of transitioning garnet from superlithiophobicity to superlithiophilicity is a promising strategy for future SSE and ASSLB designs.

RESULTS AND DISCUSSION

In this study, niobium (Nb) and calcium (Ca) codoped $Li_7La_3Zr_2O_{12}$ ($Li_{6.85}La_{2.9}Ca_{0.1}Zr_{1.75}Nb_{0.25}O_{12}$, designated as LLZ) was adopted, whereby Nb doping can stabilize the cubic phase and increase the Li-ion conductivity and Ca doping can serve as a sintering aid to densify the garnet body structure at low sintering temperatures (see more details in the experimental section of the Supporting Information). The LLZ precursor powders were synthesized by a solid-state reaction at 900 °C followed by ball milling to break up soft agglomeration. The LLZ powders were pressed into pellets and sintered at 1050 °C to yield the yellowish LLZ pellet (Figure 2a). Figure S1a displays the X-ray diffraction (XRD) patterns of

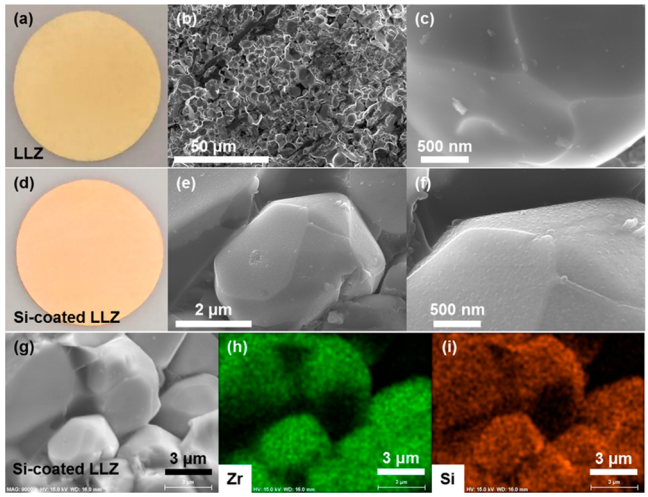

Figure 2. Coating of an ultrathin layer of amorphous Si (∼10 nm) onto a garnet solid-state electrolyte (LLZ) via PECVD. (a) Digital image of a bare LLZ pellet. (b,c) SEM images of bare LLZ at different magnifications. Crystallized LLZ particles with a smooth surface can be observed. (d) Digital image of the Si-coated LLZ, where a noticeable color change from yellow to orange occurs. (e,f) SEM images of the Si-coated LLZ, where the surface became rougher after coating. (g−i) EDX elemental mapping images of Si-coated LLZ. The elemental Zr and Si overlap well, which suggests that Si is uniformly distributed on LLZ.

the calcined precursor LLZ powder and the sintered LLZ pellet with the standard cubic phase present in the garnet structure (PDF-80-0457). The stabilized cubic phase enables a high Li-ion conductivity of 2.5×10^{-4} S/cm, as displayed in Figure S1b. The Li-ion conductivity of LLZ is also thermally activated and obeys the Arrhenius equation, where the activation energy is 0.35 eV and comparable to other reported values.[35]

Figure 2b is a low-magnification scanning electron microscopy (SEM) image of the polished LLZ pellet, showing a large quantity of crystallized particles on the order of several micrometers. The zoomed-in SEM image in Figure 2c shows the garnet's smooth surface. After coating an ultrathin layer of amorphous Si (∼10 nm) by PECVD, the LLZ turns orange (Figure 2d). High-magnification SEM images show that the LLZ surface becomes rougher after coating (Figure 2e and f). Figure 2g to 2i are energy-dispersive X-ray (EDX) elemental mapping images, where the elemental Zr signal overlaps well with elemental Si. These results verify the uniform distribution of Si on the surface of LLZ by PECVD, a well-known technique used in the semiconductor industry. Note that the surface of

DOI: 10.1021/jacs.6b06777
J. Am. Chem. Soc. 2016, 138, 12258−12262

many other SSEs can be easily modified using an inexpensive Si layer coating by PECVD.

To evaluate the wettability of LLZ before and after Si coating, we designed and fabricated an LLZ pellet with amorphous Si (~10 nm) selectively deposited on only one-half of the pellet area (Figure 3a). As shown in Figure 3d, the

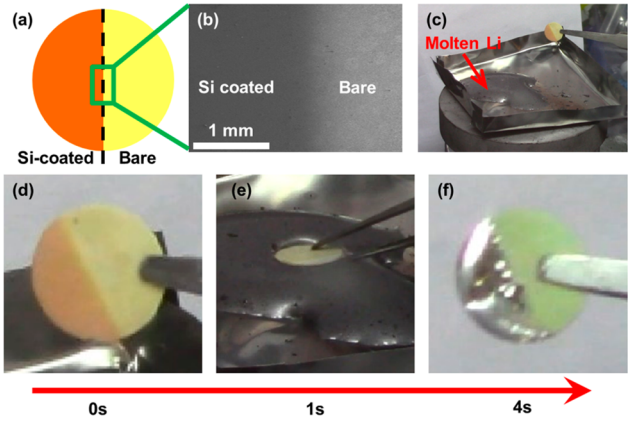

Figure 3. Evaluation of LLZ wettability with Li metal. (a) Schematic showing the designed LLZ pellet with only one half (orange) selectively coated with amorphous Si. (b) SEM image showing the contrast between the bare LLZ area and the Si-coated area. (c) A homemade setup for the wettability evaluation, where molten Li was loaded in a stainless steel boat on a hot plate (~200 °C). Digital images of the half-coated LLZ pellet before and after dipping in molten Li for (d) 0, (e) 1, and (f) 4 s. This shows the dramatic wettability transition of LLZ from superlithiophobicity to superlithiophilicity using an amorphous Si coating.

orange half denotes the Si-coated LLZ pellet area, which is further confirmed by SEM (Figure 3b) and EDX mapping observations (Figure S2). The wettability was tested by dipping this unique LLZ pellet into molten Li using a homemade setup (Figure 3c). After dipping into molten Li for only 4 s, the Si-coated side was fully coated with Li metal while the bare side remained clean (Figure 3d–f). The entire Li coating process can be found in MovieS1 of Supporting Information, where the sharp contrast between the Si-coated and bare LLZ sides indicates a dramatic wettability transition of LLZ from superlithiophobicity to superlithiophilicity due to the amorphous Si coating.

Prompted by the enhanced wettability, the interfacial resistance between the Li metal and Si-coated LLZ is expected to decrease. For the Li metal/LLZ interface resistance to be tested, LLZ or Si-coated LLZ was sandwiched by two Li metal electrodes to assemble symmetric cells (Figure 4a and b). Prior to the electrochemical measurements, all the cells were heated at ~200 °C for 20 min in a glovebox because thermal treatment promotes superior contact between Li and LLZ.[27,36] Because of the high reactivity of molten Li, lithiated Si will be formed in situ between the Li metal and the Si-coated LLZ. As shown in Figure 4c, the Nyquist plots of symmetric cells exhibit two distinct semicircles: one at high frequency and another at low frequency. The overall resistance of the LLZ (bulk and grain boundary) in an Au/LLZ/Au symmetric cell is 215 Ω cm^2 (Figure S3). The Li/LLZ/Li symmetric cell delivers a large resistance of 2064 Ω cm^2, where the interfacial resistance between Li and LLZ was calculated to be 925 Ω cm^2 (Figure S4a). The calculation details can be found in Supporting Information. Notably, the interfacial resistance between the Li

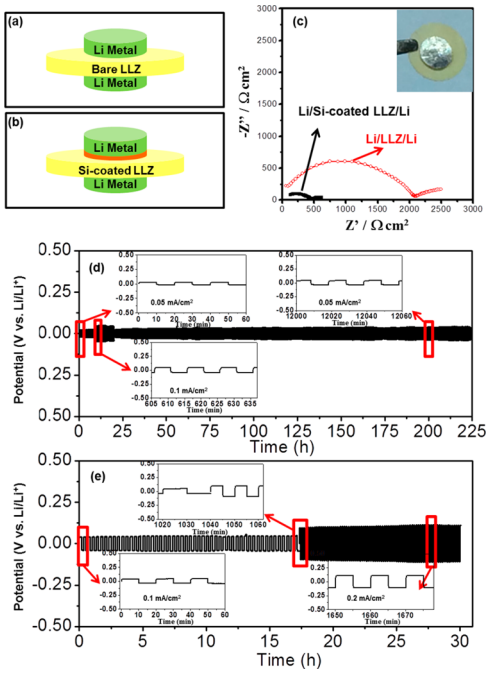

Figure 4. Electrochemical performance of symmetric cells using Si-coated and bare LLZ. Schematic illustration showing the structure of symmetric cells with (a) LLZ or (b) Si-coated LLZ SSEs. (c) Electrochemical impedance spectroscopy (EIS) measurements of symmetric cells where the interfacial resistance of the Si-coated garnet cell was significantly decreased. (inset) Digital image of a Li/Si-coated LLZ/Li symmetric cell. (d) Long-term cycling performance of the Li/Si-coated LLZ/Li symmetric cell at current densities of 0.05 and 0.1 mA/cm^2. (e) Voltage profiles of the Li/Si-coated LLZ/Li symmetric cell at current densities of 0.1 and 0.2 mA/cm^2.

and Si-coated LLZ was dramatically decreased to 127 Ω cm^2, which is approximately 7.3 times lower than bare LLZ (Figure S4b). Therefore, the improved wettability from Si coating and the in situ formation of lithiated Si led to a much smaller interfacial resistance. As expected, the cell with Si-coated LLZ delivered stable plating/stripping behavior. When the Li/Si-coated/Li cell was tested at 0.05 or 0.1 mA/cm^2, the voltage profiles exhibited flat and stable plating and stripping curves with a small overpotential (Figure 4d). After cycling for 225 h, the voltage profiles were still stable, indicating great cycling performance. As the current density was increased to 0.2 mA/cm^2, the overpotential remained small, and the cell delivered stable cycling performance (Figure 4e). However, the symmetric cell with bare LLZ exhibited a large overpotential, unstable voltage profiles, and poor cyclability (Figure S5). This is due to the large interfacial resistance between the Li metal and bare LLZ, which has been widely observed in previous studies.[26,27,34,36] For example, Kotobuki et al. reported a Li/LLZ/Li symmetric cell, which showed a large resistance of ~5500 Ω and a large overpotential during plating/striping.[36] Similarly, Janek's group demonstrated a large interfacial resistance between Li and garnet.[34] Therefore, our study proves that the Li metal/LLZ interface and the striping/plating process can be greatly improved by depositing an amorphous Si as well as the in situ formation of a lithiated Si layer.

It is well-known that the reaction between molten Li and Si is spontaneous[13,37,38] and that lithiated Si is a good Li-ion conductor ($D_{Li^+} \approx 10^{-12}$ m^2/s).[39−43] To demonstrate the Li-ion conduction of lithiated Si, we performed a simple experiment

DOI: 10.1021/jacs.6b06777
J. Am. Chem. Soc. 2016, 138, 12258−12262

where Li metal foil was adhered to Si-coated LLZ and placed on a hot plate (Figure 5a). When the Li metal started to melt at

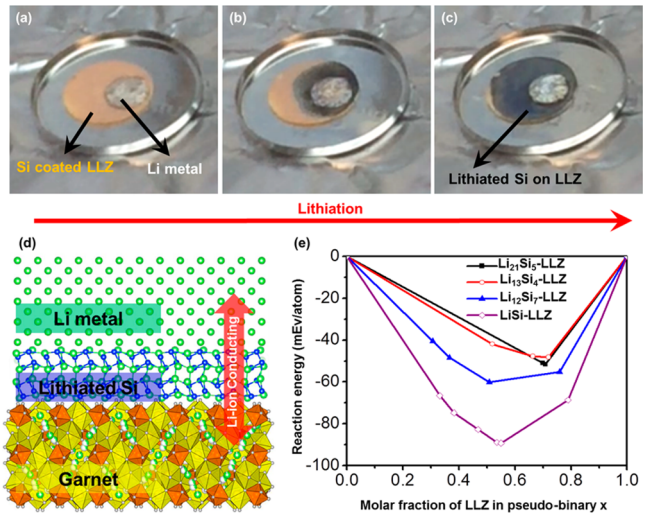

Figure 5. Structural evolution of Si-coated LLZ upon lithiation by molten Li. Digital images of Si-coated LLZ (a) before and (b,c) after lithiation, which shows the exceptional Li-ion conductivity of lithiated Si. (d) Schematic view of the superlithiophilic garnet-Li metal interface enabled by the in situ-formed, lithiated Si layer. (e) Theoretical calculations demonstrate improved interfacial contacts between LLZ and Li metal due to the enhanced wetting mediated by the in situ-lithiated Si interlayer. Mutual reaction energy of interfaces between LLZ and lithiated Si interfaces were calculated. The negative reaction energy indicates enhanced wetting and good interfacial contacts between LLZ and the in situ-formed, lithiated Si interlayer.

~190 °C, the Si-coated LLZ area near the Li metal changed color from orange to black (Figure 5b). This color change denotes the lithiation process of Si. Interestingly, the entire surface became black upon lithiation, which suggests the reaction occurred not only in areas directly in contact with Li metal but also across the entire Si-coated LLZ (Figure 5c). A detailed demonstration of this lithiation behavior can be found in MovieS2 of the Supporting Information. As demonstrated in Figure 5d, when a thin layer of Si was coated onto garnet, the in situ-formed, lithiated Si can conduct Li ions effectively between Li metal/LLZ. First-principles calculations were performed to investigate the interface stability between the LLZ and the newly formed lithiated Si. By considering the interface as a pseudobinary system of lithiated Si and LLZ, the most thermodynamically favorable phase equilibria as interphase layer were identified, and the reaction energy to form these interphases was calculated.[44] We found that the reaction energies are in the range of −90 and −40 meV/atom (Figure 5e and details in Table S1), which suggests reasonable stability of the interface between lithiated Si and LLZ. The limited interfacial reaction energy indicates potential kinetic stabilization and less interfacial degradation compared to those of other SSEs.[44,45] Additionally, the wettability at the interface is improved by the minor reactions at the interface. Therefore, the interface between lithiated Si and LLZ may exhibit both good stability and wettability, which enhances the interfacial contact and reduces the overall interfacial resistance.

CONCLUSIONS

In summary, we have developed a strategy to improve the Li metal/LLZ interface by depositing an ultrathin layer of amorphous Si via PECVD for the first time. The wettability of the LLZ dramatically changed from superlithiophobic to superlithiophilic behavior due to the reaction between Li and Si. The resulting Si-coated LLZ symmetric cells exhibit a 7-fold decrease in interfacial resistance as well as stable plating/striping processes compared to those of bare LLZ. We believe that our route to solve the interface problem between Li metal and LLZ can also be extended to other solid-state electrolytes. All solid-state Li batteries using Li metal as the anode can take advantage of these findings. Note that PECVD Si coating is a well-developed technique in the semiconductor industry, which enables a straightforward transition toward scalable, all-solid-state Li metal battery development. PECVD can also conformally deposit material within three-dimensional porous garnet networks. Therefore, this technique can facilitate more advanced cell designs with numerous garnet-based electrolytes.

ASSOCIATED CONTENT

Supporting Information

The Supporting Information is available free of charge on the ACS Publications website at DOI: 10.1021/jacs.6b06777.

Movie of the entire Li-coating process (AVI)
Movie showing a detailed demonstration of the lithiation behavior (AVI)
Conductivity of LLZ, SEM and EDX mapping images of Si-coated LLZ, Nyquist plots of cells, plating/striping performance of the Li/LLZ/Li cell, and calculation results (PDF)

AUTHOR INFORMATION

Corresponding Authors

*binghu@umd.edu.
*ewach@umd.edu.

Author Contributions

⊥W.L. and Y.G. contributed equally to this work.

Notes

The authors declare no competing financial interest.

ACKNOWLEDGMENTS

This work was funded by the U.S. Department of Energy (DOE), EERE contract #DEEE0006860 (entitled "Overcoming Interfacial Impedance in Solid-State Batteries"). We acknowledge the support of the Maryland NanoCenter and its FabLab and NispLab. We acknowledge the supercomputing resources from the University of Maryland High Performance Computing Environment, Maryland Advanced Research Computing Center (MARCC), and Extreme Science and Engineering Discovery Environment (XSEDE) under Grant No. TG-DMR130142. We thank Dr. Shaofei Wang from the University of Texas at Austin for his help and discussion on EIS analysis.

REFERENCES

(1) Whittingham, M. S. *Chem. Rev.* **2014**, *114*, 11414.
(2) Etacheri, V.; Marom, R.; Elazari, R.; Salitra, G.; Aurbach, D. *Energy Environ. Sci.* **2011**, *4*, 3243.
(3) Xu, W.; Wang, J.; Ding, F.; Chen, X.; Nasybulin, E.; Zhang, Y.; Zhang, J.-G. *Energy Environ. Sci.* **2014**, *7*, 513.
(4) Aurbach, D.; Zinigrad, E.; Cohen, Y.; Teller, H. *Solid State Ionics* **2002**, *148*, 405.

DOI: 10.1021/jacs.6b06777
J. Am. Chem. Soc. 2016, 138, 12258−12262

(5) Chang, H. J.; Ilott, A. J.; Trease, N. M.; Mohammadi, M.; Jerschow, A.; Grey, C. P. *J. Am. Chem. Soc.* **2015**, *137*, 15209.
(6) Ding, F.; Xu, W.; Graff, G. L.; Zhang, J.; Sushko, M. L.; Chen, X.; Shao, Y.; Engelhard, M. H.; Nie, Z.; Xiao, J.; Liu, X.; Sushko, P. V.; Liu, J.; Zhang, J.-G. *J. Am. Chem. Soc.* **2013**, *135*, 4450.
(7) Qian, J.; Henderson, W. A.; Xu, W.; Bhattacharya, P.; Engelhard, M.; Borodin, O.; Zhang, J.-G. *Nat. Commun.* **2015**, *6*, 6362.
(8) Zheng, G.; Lee, S. W.; Liang, Z.; Lee, H.-W.; Yan, K.; Yao, H.; Wang, H.; Li, W.; Chu, S.; Cui, Y. *Nat. Nanotechnol.* **2014**, *9*, 618.
(9) Yan, K.; Lee, H.-W.; Gao, T.; Zheng, G.; Yao, H.; Wang, H.; Lu, Z.; Zhou, Y.; Liang, Z.; Liu, Z.; Chu, S.; Cui, Y. *Nano Lett.* **2014**, *14*, 6016.
(10) Zhang, R.; Cheng, X.-B.; Zhao, C.-Z.; Peng, H.-J.; Shi, J.-L.; Huang, J.-Q.; Wang, J.; Wei, F.; Zhang, Q. *Adv. Mater.* **2016**, *28*, 2155.
(11) Ji, X.; Liu, D.-Y.; Prendiville, D. G.; Zhang, Y.; Liu, X.; Stucky, G. D. *Nano Today* **2012**, *7*, 10.
(12) Liu, Y.; Lin, D.; Liang, Z.; Zhao, J.; Yan, K.; Cui, Y. *Nat. Commun.* **2016**, *7*, 10992.
(13) Liang, Z.; Lin, D.; Zhao, J.; Lu, Z.; Liu, Y.; Liu, C.; Lu, Y.; Wang, H.; Yan, K.; Tao, X.; Cui, Y. *Proc. Natl. Acad. Sci. U. S. A.* **2016**, *113*, 2862.
(14) Luo, W.; Zhou, L.; Fu, K.; Yang, Z.; Wan, J.; Manno, M.; Yao, Y.; Zhu, H.; Yang, B.; Hu, L. *Nano Lett.* **2015**, *15*, 6149.
(15) Quartarone, E.; Mustarelli, P. *Chem. Soc. Rev.* **2011**, *40*, 2525.
(16) Takada, K. *Acta Mater.* **2013**, *61*, 759.
(17) McCloskey, B. D. *J. Phys. Chem. Lett.* **2015**, *6*, 4581.
(18) Monroe, C.; Newman, J. *J. Electrochem. Soc.* **2005**, *152*, A396.
(19) Ni, J. E.; Case, E. D.; Sakamoto, J. S.; Rangasamy, E.; Wolfenstine, J. B. *J. Mater. Sci.* **2012**, *47*, 7978.
(20) Kamaya, N.; Homma, K.; Yamakawa, Y.; Hirayama, M.; Kanno, R.; Yonemura, M.; Kamiyama, T.; Kato, Y.; Hama, S.; Kawamoto, K.; Mitsui, A. *Nat. Mater.* **2011**, *10*, 682.
(21) Liu, Z.; Fu, W.; Payzant, E. A.; Yu, X.; Wu, Z.; Dudney, N. J.; Kiggans, J.; Hong, K.; Rondinone, A. J.; Liang, C. *J. Am. Chem. Soc.* **2013**, *135*, 975.
(22) Bron, P.; Johansson, S.; Zick, K.; Schmedt auf der Günne, J.; Dehnen, S.; Roling, B. *J. Am. Chem. Soc.* **2013**, *135*, 15694.
(23) Kato, Y.; Hori, S.; Saito, T.; Suzuki, K.; Hirayama, M.; Mitsui, A.; Yonemura, M.; Iba, H.; Kanno, R. *Nat. Energy* **2016**, *1*, 16030.
(24) Thangadurai, V.; Kaack, H.; Weppner, W. J. F. *J. Am. Ceram. Soc.* **2003**, *86*, 437.
(25) Murugan, R.; Thangadurai, V.; Weppner, W. *Angew. Chem., Int. Ed.* **2007**, *46*, 7778.
(26) Tsai, C.-L.; Roddatis, V.; Chandran, C. V.; Ma, Q.; Uhlenbruck, S.; Bram, M.; Heitjans, P.; Guillon, O. *ACS Appl. Mater. Interfaces* **2016**, *8*, 10617.
(27) Buschmann, H.; Dolle, J.; Berendts, S.; Kuhn, A.; Bottke, P.; Wilkening, M.; Heitjans, P.; Senyshyn, A.; Ehrenberg, H.; Lotnyk, A.; Duppel, V.; Kienle, L.; Janek, J. *Phys. Chem. Chem. Phys.* **2011**, *13*, 19378.
(28) Luntz, A. C.; Voss, J.; Reuter, K. *J. Phys. Chem. Lett.* **2015**, *6*, 4599.
(29) Ohta, N.; Takada, K.; Zhang, L.; Ma, R.; Osada, M.; Sasaki, T. *Adv. Mater.* **2006**, *18*, 2226.
(30) Thangadurai, V.; Narayanan, S.; Pinzaru, D. *Chem. Soc. Rev.* **2014**, *43*, 4714.
(31) Narayanan, S.; Ramezanipour, F.; Thangadurai, V. *Inorg. Chem.* **2015**, *54*, 6968.
(32) Kato, T.; Hamanaka, T.; Yamamoto, K.; Hirayama, T.; Sagane, F.; Motoyama, M.; Iriyama, Y. *J. Power Sources* **2014**, *260*, 292.
(33) Du, F.; Zhao, N.; Li, Y.; Chen, C.; Liu, Z.; Guo, X. *J. Power Sources* **2015**, *300*, 24.
(34) Buschmann, H.; Berendts, S.; Mogwitz, B.; Janek, J. *J. Power Sources* **2012**, *206*, 236.
(35) Sharafi, A.; Meyer, H. M.; Nanda, J.; Wolfenstine, J.; Sakamoto, J. *J. Power Sources* **2016**, *302*, 135.
(36) Kotobuki, M.; Munakata, H.; Kanamura, K.; Sato, Y.; Yoshida, T. *J. Electrochem. Soc.* **2010**, *157*, A1076.
(37) Dębski, A.; Gąsior, W.; Góral, A. *Intermetallics* **2012**, *26*, 157.
(38) Li, H.; Huang, X.; Chen, L.; Zhou, G.; Zhang, Z.; Yu, D.; Jun, M. Y.; Pei, N. *Solid State Ionics* **2000**, *135*, 181.
(39) Pollak, E.; Salitra, G.; Baranchugov, V.; Aurbach, D. *J. Phys. Chem. C* **2007**, *111*, 11437.
(40) McDowell, M. T.; Cui, Y. *Adv. Energy Mater.* **2011**, *1*, 894.
(41) Zhao, K.; Tritsaris, G. A.; Pharr, M.; Wang, W. L.; Okeke, O.; Suo, Z.; Vlassak, J. J.; Kaxiras, E. *Nano Lett.* **2012**, *12*, 4397.
(42) Pharr, M.; Zhao, K.; Wang, X.; Suo, Z.; Vlassak, J. J. *Nano Lett.* **2012**, *12*, 5039.
(43) Ding, N.; Xu, J.; Yao, Y. X.; Wegner, G.; Fang, X.; Chen, C. H.; Lieberwirth, I. *Solid State Ionics* **2009**, *180*, 222.
(44) Zhu, Y.; He, X.; Mo, Y. *J. Mater. Chem. A* **2016**, *4*, 3253.
(45) Zhu, Y.; He, X.; Mo, Y. *ACS Appl. Mater. Interfaces* **2015**, *7*, 23685.

DOI: 10.1021/jacs.6b06777
J. Am. Chem. Soc. 2016, 138, 12258−12262